Nonperturbative terahertz electro-optics of semiconductor quantum wells in strong magnetic fields

2001 J. Phys.: Condens. Matter 13 10979

(http://iopscience.iop.org/0953-8984/13/48/322)

INSTITUTE OF PHYSICS PUBLISHING JOURNAL OF PHYSICS: CONDENSED MATTER

J. Phys.: Condens. Matter **13** (2001) 10979–10990 PII: S0953-8984(01)26849-0

Nonperturbative terahertz electro-optics of semiconductor quantum wells in strong magnetic fields

Takeshi Inoshita

ERATO, JST, NTT Atsugi R&D Centre 4S-308S, 3-1 Morinosato Wakamiya, Atsugi 243-0198, Japan

Received 6 July 2001
Published 16 November 2001
Online at stacks.iop.org/JPhysCM/13/10979

Abstract

A theory for the absorption and scattering (sideband generation) of near-infrared light by undoped quantum wells subjected to intense terahertz radiation and a quantizing magnetic field is presented. It is based on rigorous stationary wave functions for Landau levels driven by an alternating-current field. Due to their characteristic energy structure, the response of Landau levels to the terahertz radiation diverges at cyclotron resonance. This singularity, absent in the conventional optical Stark effect of atoms, leads to the disappearance of both absorption and sideband intensities (terahertz-induced transparency) at resonance or in the limit of strong terahertz intensity.

1. Introduction

In the last decade, the need for broad-band communication systems has heightened interest in terahertz electro-optics. Nonlinear optical phenomena, such as THz sideband generation [1–8] and the Franz–Keldysh effect [9–14], both discovered recently, are expected to play key roles in the realization of such systems. In a previous publication, I have proposed a perturbation theory for resonant THz sideband generation (i.e., sum and difference frequency generation involving one near-infrared photon and multiple THz photons) in undoped semiconductor quantum wells in strong magnetic fields [15, 16]. The susceptibility obtained, assuming both the near-infrared (NIR) and THz fields to be small, can successfully explain the experiment.

In the present paper, I extend this theory to the regime of stronger THz fields and discuss both absorption and sideband generation. (Preliminary results for sideband generation were reported in references [17] and [18].) The theory treats the THz field nonperturbatively, while the NIR field is considered as a small perturbation. Both fields are assumed to be switched on adiabatically, so transient effects are beyond the scope of the present paper. We approach the problem by examining (1) how the Landau levels (LLs) are dressed by the THz radiation (optical Stark effect) and (2) how the THz-dressed LLs scatter and absorb the NIR light. These are discussed separately in sections 2 and 3, respectively. Numerical results are discussed in section 4, and a summary is given in section 5.

0953-8984/01/4810979+12$30.00

2. Intraband dynamics of Landau levels driven by terahertz radiation

The system that we consider is an undoped semiconductor multiple quantum well at $T = 0$ (growth axis $\parallel \boldsymbol{z}$) driven by intense THz radiation, linearly polarized in the well plane, in a quantizing magnetic field $\boldsymbol{B} = (0, 0, B)$. The sample is taken to be a thin rectangular slab with side lengths L_x, L_y, and L_z. We assume that the barriers between the wells are high/thick enough that the wave-function overlap between the wells is negligible. Furthermore, we only consider the case of small well width where the orbital degeneracy of the heavy and light valence bands is completely lifted [19]. This allows us to use a single-band parabolic approximation for both the conduction band (CB) and valence band (VB) (mass $m_c > 0$ and $-m_v < 0$, respectively). Since the NIR light, causing interband transitions, is weak by assumption, we neglect electron–electron interactions. Electron–hole interactions (exciton effects) are also negligible if the magnetic energy is much larger than the exciton binding energy: $eB/\mu c \gg \mu e^4/2\epsilon^2$, where $\mu = (m_c^{-1} + m_v^{-1})^{-1}$, $e > 0$ is the elementary charge, c is the light velocity in vacuum, ϵ is the static dielectric constant, and we set $\hbar$ equal to 1. For GaAs, this condition is satisfied if $B \gg 1$ T. We limit our discussion to this regime.

Disregarding the NIR light for the moment and assuming that the THz field is not so strong as to induce interband transitions, let us first examine the stationary dynamics of an electron in the CB driven by the THz field. Writing the THz electric field as $\boldsymbol{E}_{\rm THz} = (E_{\rm THz}, 0, 0) \sin \omega t$ and choosing the vector potential of the magnetic field as $\boldsymbol{A} = (0, Bx, 0)$, the Hamiltonian H can be written as

$$H = \frac{1}{2m_c}\left(p_x^2 + p_y^2 + \frac{2eB}{c}p_y x + \frac{e^2B^2}{c^2}x^2\right) + eE_{\rm THz}x \sin \omega t \tag{1}$$

where $\boldsymbol{p} = (p_x, p_y)$ is the electron momentum. Before examining the quantum dynamics of the system, let us look at the classical electron motion. The classical equation of motion derived from this Hamiltonian has the following stationary solutions:

$$x = \tilde{X}(t) + a\cos(\omega_c t + \theta) \tag{2a}$$

$$y = \tilde{Y}(t) + a\sin(\omega_c t + \theta) \tag{2b}$$

with

$$\tilde{X}(t) = X + \frac{eE_{\rm THz}}{m_c(\omega^2 - \omega_c^2)}\sin(\omega t) \tag{3a}$$

$$\tilde{Y}(t) = Y + \frac{eE_{\rm THz}}{m_c(\omega^2 - \omega_c^2)}\frac{\omega_c}{\omega}[1 - \cos(\omega t)]. \tag{3b}$$

Here a and $\omega_c = eB/m_c c$ are the cyclotron radius and frequency, respectively, $[\tilde{X}(t), \tilde{Y}(t)]$ is the cyclotron centre, and θ, X, and Y are constants. Equations (3) show that $(\tilde{X}, \tilde{Y})$ revolves along an elliptic orbit with frequency ω. It is to be noted that both the major and minor radii of the orbit are $\propto E_{\rm THz}/|\omega^2 - \omega_c^2|$.

Turning to the quantum dynamics, it can be described, in the effective-mass approximation, by the following Schrödinger equation for the envelope function $\psi_c(x, y, t)$:

$$\mathrm{i}\frac{\partial \psi_c}{\partial t} = H\psi_c. \tag{4}$$

Let us put

$$\psi_c(x, y, t) = L_y^{-1/2}\exp[-\mathrm{i}eBXy/c + \mathrm{i}eE_{\rm THz}X\omega^{-1}\cos\omega t]\phi_c(x - X, t).$$

Here $X = 2\pi\ell^2 n/L_y$, with n being an integer in the range $-L_xL_y/4\pi\ell^2 < n < L_xL_y/4\pi\ell^2$ and $\ell = \sqrt{c/Be}$ (magnetic length). This reduces the problem to that of a driven harmonic oscillator:

$$\mathrm{i}\frac{\partial\phi_c}{\partial t} = -\frac{1}{2m_c}\frac{\partial^2\phi_c}{\partial x^2} + \frac{m_c}{2}\omega_c^2 x^2\phi_c + eE_{\mathrm{THz}}x\sin(\omega t)\phi_c. \tag{5}$$

As shown in appendix A, the stationary solutions of equation (5) can be written as

$$\phi_{cn}(x,t) = w_{cn}(x-\gamma_c)\exp\left(-\mathrm{i}E_{cn}t + \mathrm{i}m_c\dot{\gamma}_c(x-\gamma_c) + \mathrm{i}\int_0^t L_c(s)\,\mathrm{d}s\right) \tag{6}$$

where $w_{cn}(x)$ is the nth normalized harmonic oscillator eigenfunction with energy $E_{cn} = \omega_c(n+1/2)$ $(n = 0, 1, 2, \ldots)$, $\gamma_c(t) = eE_{\mathrm{THz}}/m_c(\omega^2-\omega_c^2)\sin\omega t$ is a classical trajectory, $L_c(t) = m_c\dot{\gamma_c}^2/2 - m_c\omega_c^2\gamma_c^2 - eE_{\mathrm{THz}}\gamma_c\sin\omega t$ is the Lagrangian for $\gamma_c(t)$, and $\dot{\gamma}_c = \mathrm{d}\gamma_c/\mathrm{d}t$. Combining all these, we get the following solutions of equation (4) [20]:

$$\psi_{cnX}(x,y,t) = \frac{1}{\sqrt{L_y}}w_{cn}(x-X-\gamma_c)\mathrm{e}^{-\mathrm{i}\bar{E}_{cn}t - \mathrm{i}Xy/\ell^2 + \mathrm{i}G_{cX}} \tag{7a}$$

$$G_{cX}(xt) = \left[\frac{eE_{\mathrm{THz}}X}{\omega} + \frac{eE_{\mathrm{THz}}(x-X)\omega}{\omega^2-\omega_c^2}\right]\cos\omega t - \frac{e^2E_{\mathrm{THz}}^2(\omega^2+\omega_c^2)}{8m_c\omega(\omega^2-\omega_c^2)^2}\sin 2\omega t \tag{7b}$$

$$\bar{E}_{cn} = E_G + \left(n+\frac{1}{2}\right)\omega_c + \frac{e^2E_{\mathrm{THz}}^2}{4m_c(\omega^2-\omega_c^2)} \tag{7c}$$

where $n = 0, 1, 2, \ldots$. Since we hereafter measure electron energy relative to the VB edge, the band gap E_G is included in $\bar{E}_{cn}$.

It is well known that in the static case ($E_{\mathrm{THz}} = 0$), the Landau index n and the centre coordinate X can be chosen as quantum numbers [21]. Equations (7) show that even when $E_{\mathrm{THz}} \neq 0$, $X = \tilde{X}(0)$ can be used to label stationary wave functions.

The above discussion of the CB electron dynamics can be easily adapted to the VB: we merely have to replace m_c by $-m_v$. The result is

$$\psi_{vnX}(x,y,t) = \frac{1}{\sqrt{L_y}}w_{vn}(x-X-\gamma_v)\mathrm{e}^{-\mathrm{i}\bar{E}_{vn}t - \mathrm{i}Xy/\ell^2 + \mathrm{i}G_{vX}} \tag{8a}$$

$$G_{vX}(xt) = \left[\frac{eE_{\mathrm{THz}}X}{\omega} + \frac{eE_{\mathrm{THz}}(x-X)\omega}{\omega^2-\omega_v^2}\right]\cos\omega t + \frac{e^2E_{\mathrm{THz}}^2(\omega^2+\omega_v^2)}{8m_v\omega(\omega^2-\omega_v^2)^2}\sin 2\omega t \tag{8b}$$

$$\bar{E}_{vn} = -\left(n+\frac{1}{2}\right)\omega_v - \frac{e^2E_{\mathrm{THz}}^2}{4m_v(\omega^2-\omega_v^2)} \tag{8c}$$

where $\gamma_v(t) = -eE_{\mathrm{THz}}/m_v(\omega^2-\omega_v^2)\sin\omega t$ and $\omega_v = eB/m_vc$.

It is seen from equations (7) and (8) that $\psi_{cnX}(xyt)$ and $\psi_{vnX}(xyt)$ have temporal Fourier components $\bar{E}_{cn} + l\omega$ and $\bar{E}_{vn} + l\omega$, respectively, where l is an integer, i.e., the LLs split into THz sidebands. Moreover, the second term of $\bar{E}_{cn}$ (or $\bar{E}_{vn}$) indicates that the THz field induces a rigid (i.e., independent of n and l) shift of these photon sidebands. This shift changes sign and diverges at ω_c. This rigid shift of all the levels, leaving their separation ω_c unchanged, is quite distinct from the conventional optical Stark effect of atoms [22]. For atoms, it is a good approximation to single out a few pairs of levels that are nearly resonant with the field. The field renormalizes the level separations in such a way that no singularity arises. This simple dressed-atom picture fails for LLs, where the level separation is not affected by the field. The resonant singularity persists, and the dynamic response of the LLs diverges at resonance. As we will see, this singularity leads to novel electro-optic effects.

The stationary wave functions $\psi_{cnX}(xyt)$, $\psi_{vnX}(xyt)$ are orthonormal and complete:

$$\langle\psi_{\kappa nX}(t)|\psi_{\kappa' n' X'}(t)\rangle \equiv \int \psi^*_{\kappa nX}(xyt)\psi_{\kappa' n' X'}(xyt)\,\mathrm{d}x\,\mathrm{d}y = \delta_{\kappa\kappa'}\delta_{nn'}\delta_{XX'} \tag{9a}$$

$$\sum_{nX} \psi^*_{\kappa nX}(xyt)\psi_{\kappa nX}(x'y't) = \delta(x-x')\delta(y-y') \tag{9b}$$

where $\kappa = c$ or v. Without THz radiation, all the VB LLs are occupied and CB LLs are empty. As the THz field is switched on adiabatically, these states evolve into $\psi_{vnX}(t)$ and $\psi_{cnX}(t)$, respectively, so we finally have all the $\psi_{cnX}(t)$ occupied and all the $\psi_{vnX}(t)$ empty. Now we switch on the NIR light slowly, inducing transitions between $\psi_{vnX}(t)$ and $\psi_{cnX}(t)$. This interband process is discussed in the next section.

3. Absorption and scattering of NIR radiation

For a sinusoidal NIR field $\boldsymbol{E}_{NIR}(t) = (E_{0x}, E_{0y}, 0)\sin(\Omega t + \phi)$, where ϕ is the phase difference between the THz and NIR fields, the Hamiltonian describing its interaction with an electron can be written as

$$H_{NIR}(t) = \frac{e}{m_0 c}\boldsymbol{A}_{NIR}(t)\cdot\boldsymbol{p} = \frac{e(\boldsymbol{E}_0\cdot\boldsymbol{p})}{m_0\Omega}\cos(\Omega t+\phi) \tag{10}$$

where $\boldsymbol{A}_{NIR}$ is the vector potential for the NIR field and m_0 the bare electron mass. Since the NIR field is weak by assumption, we treat it in the lowest order of perturbation theory. To discuss interband transitions, we need the full wave functions, including the Bloch parts, instead of the envelope functions used in the last section. The band-edge (Γ-point) Bloch functions are of the form $|S\rangle|\uparrow\rangle$ and $|S\rangle|\downarrow\rangle$ for the CB and $-(|X\rangle+\mathrm{i}|Y\rangle)|\uparrow\rangle/\sqrt{2}$ and $(|X\rangle-\mathrm{i}|Y\rangle)|\downarrow\rangle/\sqrt{2}$ for the VB [23]. Here $|S\rangle$ and $\{|X\rangle, |Y\rangle, |Z\rangle\}$ are normalized cell-periodic functions transforming like atomic s and p functions under the tetrahedral group at the Γ point, and $|\uparrow\rangle$ and $|\downarrow\rangle$ denote spin-up and spin-down functions[1] of spin 1/2. Writing these Bloch functions as $\Phi_{c\sigma}(\boldsymbol{r})$ and $\Phi_{v\sigma}(\boldsymbol{r})$ with $\sigma = 1$ (-1) for spin up (down), the full wave functions can be expressed as

$$\tilde{\psi}_{\kappa nX\sigma}(x,y,z,t) = \psi_{\kappa nX\sigma}(x,y,t)\zeta(z)\Phi_{\kappa\sigma}(x,y,z). \tag{11}$$

Here $\kappa = c$ or v, and we took into account only the ground subband of a well (envelope function $\zeta(z)$) in the z-direction, neglecting all higher subbands (strong confinement).

Starting from $\tilde{\psi}_{vnX\sigma}(x,y,z,t)$ at $t = T$ (long ago), and turning on the NIR field slowly, the wave function at $t \gg T$, to first order in H_{NIR}, can be written as $\tilde{\psi}_{vnX\sigma} + \delta\tilde{\psi}_{nX\sigma}$ with

$$\delta\tilde{\psi}_{nX\sigma}(t) = -\mathrm{i}\sum_{n',X'}\tilde{\psi}_{cn'X'\sigma}(t)\lim_{T\to-\infty}\int_T^t \mathrm{d}s\ \langle\tilde{\psi}_{cn'X'\sigma}(s)|H_{NIR}(s)|\tilde{\psi}_{vnX\sigma}(s)\rangle \mathrm{e}^{\epsilon s} \tag{12}$$

where $\mathrm{e}^{\epsilon s}$ ($\epsilon > 0$) was inserted to ensure slow switching of the NIR field. ($\epsilon \to 0$ corresponds to the adiabatic limit.) The interband current induced is

$$\boldsymbol{j}(t) = -\frac{N_w e}{L_x L_y}\sum_{nX\sigma}\langle\tilde{\psi}_{vnX\sigma}(t)|\boldsymbol{v}|\delta\tilde{\psi}_{nX\sigma}(t)\rangle + \text{c.c.} \tag{13a}$$

$$\approx -\frac{N_w e}{m_0 L_x L_y}\sum_{nX\sigma}\langle\tilde{\psi}_{vnX\sigma}(t)|\boldsymbol{p}|\delta\tilde{\psi}_{nX\sigma}(t)\rangle + \text{c.c.} \tag{13b}$$

$$= -\frac{N_w B e^2}{2\pi c m_0}\sum_{n\sigma}\langle\tilde{\psi}_{vn(X)\sigma}(t)|\boldsymbol{p}|\delta\tilde{\psi}_{n(X)\sigma}(t)\rangle + \text{c.c.} \tag{13c}$$

[1] The kets $|X\rangle$ and $|Y\rangle$ should not be confused with the cyclotron centre coordinates X and Y.

where N_w is the number of quantum wells per unit thickness. In equation (13b), we neglected the small B-dependent part of the velocity operator $\boldsymbol{v}$. (The same approximation was implicit in the use of the interaction Hamiltonian equation (10).) Since, as shown in appendix B, $\langle\tilde{\psi}_{vnX\sigma}(t)|\boldsymbol{p}|\delta\tilde{\psi}_{nX\sigma}(t)\rangle$ is independent of X, the Xs in the matrix element of equation (13c) were put in parentheses and the X-summation was carried out explicitly.

Combining equations (10), (12), and (13c), we obtain the α-component ($\alpha = x, y$) of $\boldsymbol{j}$ as

$$j_\alpha(t) = \frac{\mathrm{i}N_w Be^3}{2\pi cm_0^2\Omega}\sum_{nn'\sigma\beta} E_{0\beta}Q^*_{nn'\sigma,\alpha}(t)\int_{-\infty}^{t}\mathrm{d}t'\; Q_{nn'\sigma,\beta}(t')\cos(\Omega t'+\phi)\mathrm{e}^{\epsilon t'} + c.c. \tag{14}$$

where $Q_{nn'\sigma,\alpha}(t) = \langle\tilde{\psi}_{cn(X)\sigma}(t)|p_\alpha|\tilde{\psi}_{vn'(X)\sigma}(t)\rangle$. The explicit form of $Q_{nn'\sigma,\alpha}$ is obtained in appendix B:

$$Q_{nn'\sigma,\alpha} = \langle\Phi_{c\sigma}|p_\alpha|\Phi_{v\sigma}\rangle\mathrm{e}^{\mathrm{i}(\bar{E}_{cn}-\bar{E}_{vn'})t}\sum_{l=-\infty}^{\infty}{}^{(n-n')}\mathrm{e}^{-\mathrm{i}l\omega t}D(l,n,n') \tag{15}$$

where $D(l,n,n')$ is a function of ω, E_{THz}, and B (see equations (B.5)), and the l-summation runs over even (odd) integers if $n-n'$ is even (odd). Using this expression, $j_\alpha(t)$ can be expressed as a sum over sidebands:

$$j_\alpha(t) = \sum_{l=-\infty}^{\infty}(\Omega+2l\omega)\sum_\beta\left[(\chi_{2l})_{\alpha\beta}\mathrm{e}^{-\mathrm{i}(\Omega+2l\omega)t-\mathrm{i}\phi} + (\chi_{2l})^*_{\alpha\beta}\mathrm{e}^{\mathrm{i}(\Omega+2l\omega)t+\mathrm{i}\phi}\right]E_{0\beta}. \tag{16}$$

Here the tensors χ_l are

$$(\chi_l)_{\alpha\beta} = \frac{N_w Be^3}{4\pi(\Omega+l\omega)cm_0^2\Omega}\sum_{n,n'=0}^{\infty}\sum_{l'=-\infty}^{\infty}{}^{(n-n')}\left[\frac{S_{\alpha\beta}D(l+l',n,n')^*D(l',n,n')}{\Omega-l'\omega+\Delta_{nn'}+\mathrm{i}\epsilon}\right.$$
$$\left. - \frac{S^*_{\alpha\beta}D(l',n,n')^*D(l+l',n,n')}{\Omega+(l+l')\omega-\Delta_{nn'}+\mathrm{i}\epsilon}\right] \tag{17}$$

where

$$\Delta_{nn'} = \bar{E}_{cn} - \bar{E}_{vn'} \qquad S_{\alpha\beta} = \sum_{\sigma=\pm}\langle\Phi_{c\sigma}|p_\alpha|\Phi_{v\sigma}\rangle\langle\Phi_{v\sigma}|p_\beta|\Phi_{c\sigma}\rangle.$$

Since $\Omega - l'\omega$, $\Omega + (l+l')\omega \approx E_G \approx \Delta_{nn'}$, the first term on the right-hand side (counter-rotating-wave term) is much smaller than the second (rotating-wave term) and can safely be neglected. Equation (17) shows that only even-order sidebands are generated, which is due to the inversion symmetry of the unperturbed system in the (x, y) plane. Using $\langle\Phi_{v\sigma}|p_\alpha|\Phi_{c\sigma}\rangle = -\mathrm{i}\sigma P/\sqrt{2}$ for $\alpha = x$ and $P/\sqrt{2}$ for $\alpha = y$, where $P = -\mathrm{i}\langle X|p_x|S\rangle = -\mathrm{i}\langle Y|p_y|S\rangle$ [23], we get $S_{\alpha\beta} = P^2\delta_{\alpha\beta}$. Therefore $(\chi_l)_{xx} = (\chi_l)_{yy}$ and $(\chi_l)_{xy} = (\chi_l)_{yx} = 0$. We shall hereafter denote the diagonal elements of $(\chi_l)_{\alpha\beta}$ simply as χ_l, the final form of which reads

$$\chi_l = -\frac{P^2N_w Be^3}{4\pi(\Omega+l\omega)cm_0^2\Omega}\sum_{n,n'=0}^{\infty}\sum_{l'=-\infty}^{\infty}{}^{(n-n')}\frac{D(-l'-l,n,n')^*D(-l',n,n')}{\Omega-l'\omega-\Delta_{nn'}+\mathrm{i}\epsilon}. \tag{18}$$

χ_l is resonantly enhanced when $\Omega = \Delta_{nn'} + l\omega \equiv \Omega_{nn'l}$ where l is an even (odd) integer when $n-n'$ is even (odd). These resonances produce peaks in interband absorption spectra. Note that the peak positions $\Omega_{nn'l}$ shift with E_{THz}.

It is to be noted that more than one term under the summation may become simultaneously resonant. For example, if $\omega = (\omega_c+\omega_v)/2$, $\Omega_{nn,-2n}$ are independent of n and so Ω may be tuned to all of them. This type of resonance has already been discussed in our perturbation calculation [15, 16].

One can readily show that χ_l is an analogue of the standard susceptibility. For example, the absorption rate of the NIR light energy per unit volume is

$$\overline{\boldsymbol{j}(t)\cdot\boldsymbol{E}_{NIR}(t)} = (\mathrm{Im}\,\chi_0)\Omega E_0^2 \tag{19}$$

where the overline denotes long-time averaging. Thus, Im χ_0 gives the absorption rate of the NIR radiation, whereas $|\chi_l|$ ($l = \pm 2, \pm 4, \ldots$) gives the intensity of the lth sideband. As seen from equation (18), χ_l is independent of the phase difference ϕ between the THz and NIR beams.

4. Numerical results

Equation (18) was evaluated numerically using the standard parameters for GaAs: $m_c/m_0 = 0.067$, $m_v/m_0 = 0.11$, $N_w = 4 \times 10^5$ cm^{-1} (superlattice period = 25 nm), and $P = 1.29 \times 10^{-19}$ g cm s^{-1}. The imaginary part ϵ in the denominator takes account of relaxation (interband + intraband) through $\epsilon = 1/2\tau_{rel}$ where τ_{rel} is the phase relaxation time. All the results that we discuss below are obtained using $\epsilon = 1$ meV ($\tau_{rel} = 0.3$ ps).

Figure 1 presents the B-dependence of Im χ_0 calculated for $E_{\mathrm{THz}} = 1$ (solid line) and 10 kV cm^{-1} (dashed line), respectively. Here $\omega = 15$ meV, and Ω is tuned to Ω_{000} at each value of B. The solid line shows an overall increase $\sim B$. This quasilinear increase results from the prefactor of equation (18), i.e., LL degeneracy. At a cyclotron resonance (CR) ($\omega = \omega_c, \omega_v$), Im χ_0 is seen to drop sharply to 0. This remarkable behaviour becomes more pronounced as E_{THz} increases (dashed line): the dip extends over a wider range of B. This is a nonperturbative effect, not accounted for by a perturbation treatment of the THz field. To understand this, note first that in discussing electron–hole recombination, it suffices to consider an electron–hole pair with the same X (equation (B.2)). The distance R between their classical cyclotron centres is

$$R = \sqrt{[\tilde{X}_c(t) - \tilde{X}_v(t)]^2 + [\tilde{Y}_c(t) - \tilde{Y}_v(t)]^2} \propto \frac{E_{\mathrm{THz}}}{|\omega - \omega_{c,v}|} \qquad (\omega \approx \omega_c, \omega_v) \tag{20}$$

which diverges at CR, causing the interband transition matrix element to vanish exponentially. This resonant electron–hole separation (REHS) is a manifestation of the peculiar optical Stark effect of LLs, where the field-induced dressing of the LLs does not remove the resonant divergence.

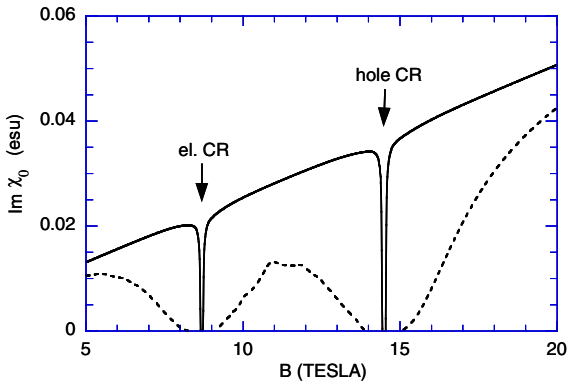

Figure 1. Calculated Im χ_0 versus B for a GaAs multiple quantum well with period 25 nm. The solid and dashed lines correspond to $E_{\mathrm{THz}} = 1$ and 10 kV cm^{-1}, respectively. Ω is tuned to the Ω_{000} resonance at each value of B. The other parameters are $\omega = 15$ meV and $\epsilon = 1$ meV.

The REHS has a significant effect on the sidebands as well. Figure 2 plots the B-dependence of $|\chi_n|$ for various sidebands ($n = \pm 2, \pm 4$) calculated with the same parameters as for figure 1. While the perturbation calculation [15, 16] displays simple peaks at CR, our nonperturbative result shows a sharp dip at the centre of each CR peak. These sharp structures, which also broaden as E_{THz} increases (dashed line), are also caused by the REHS. Unlike for the case of absorption (figure 1), the sideband intensity away from the CRs is generally enhanced by orders of magnitude by the THz field as seen by comparing the solid and dashed lines. This enhancement is not monotonic as will be discussed later.

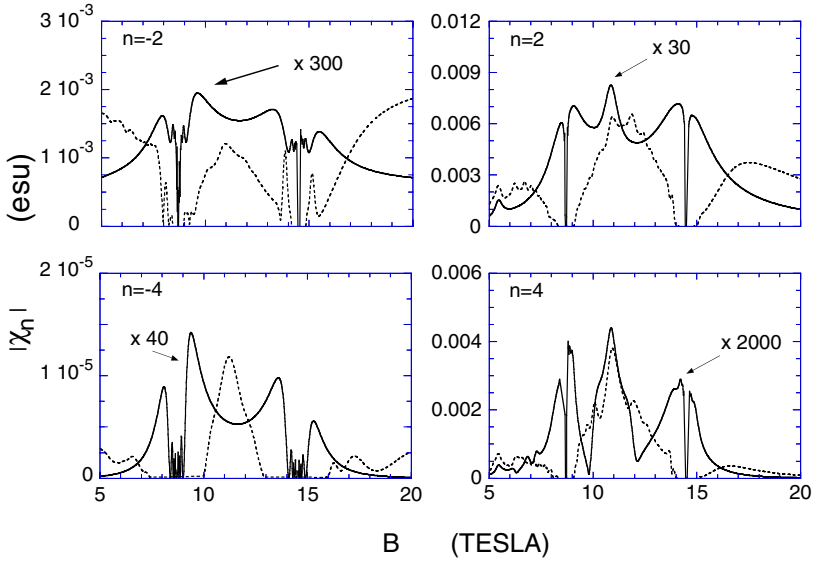

Figure 2. $|\chi|$ versus B for various sidebands obtained using the same parameters as for figure 1. The solid and dashed lines correspond to $E_{\mathrm{THz}} = 1$ and 10 kV cm^{-1}, respectively.

In addition to the two CR peaks, figure 2 ($n = 2$ and $n = 4$) displays a third peak located at $B = 10.9$ T. This results from the resonance $\omega = (\omega_c + \omega_v)/2$, the mechanism of which was discussed in the last section. Unlike the CR peaks, this peak (originating from the resonant denominators in equation (18)) is unaffected by the REHS and has no dip at its centre. Although equation (18) generally has an infinite number of resonances, only those producing the $\omega = (\omega_c + \omega_v)/2$ peak are dominant at $E_{\mathrm{THz}} = 1$ kV cm^{-1} (solid line). With increasing E_{THz}, other terms begin to contribute, generating fine subsidiary peaks (dashed line).

The E_{THz}-dependences of the absorption and sideband intensities are plotted in figures 3 and 4, respectively, for $B = 8$ T ($\omega_c = 13.81$ meV, $\omega_v = 8.28$ meV). The solid and dashed lines denote the results for $\omega = 15$ (large detuning from ω_c) and 14.5 meV (small detuning), respectively. Ω is set equal to Ω_{110} at each value of E_{THz}. As E_{THz} increases, all the plots show the general trend of oscillatory variation followed by eventual exponential drop to 0. The exponential decay (field-induced transparency) can be explained again by the REHS. The THz field drives the electron and hole cyclotron centres in different directions, pulling them apart and reducing their recombination probability. Mathematically, the REHS is represented by

$$D(l, n, n') \propto \mathrm{e}^{-(\Delta^2+\omega^2\Gamma^2)/8}$$

(equation (B.5b)) where $|\Delta|, |\Gamma| \propto E_{\mathrm{THz}}/|\omega - \omega_{c,v}|$ near a CR (equations (B.5f) and (B.5g)). Thus the threshold field strength E_{th} at which $|\chi_n|$ decays scales as the smaller of $|\omega - \omega_c|$ and

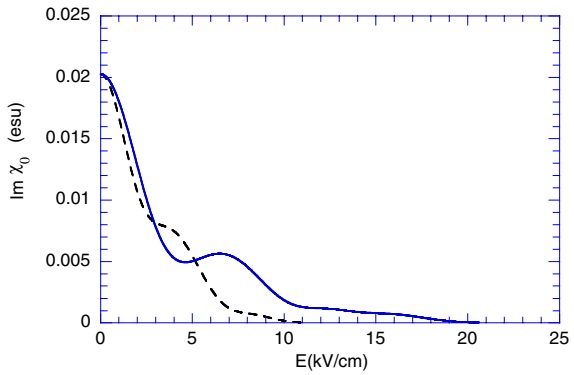

Figure 3. Calculated Im χ_0 versus E_{THz} for a GaAs multiple quantum well with period 25 nm. The solid and dashed lines represent results for $\omega = 15$ (large detuning from the electron CR, $\omega_c = 13.81$ meV) and 14.5 meV (small detuning), respectively. The other parameters are $B = 8$ T, $\epsilon = 1$ meV, and Ω is tuned to the Ω_{110} resonance at each value of E_{THz}.

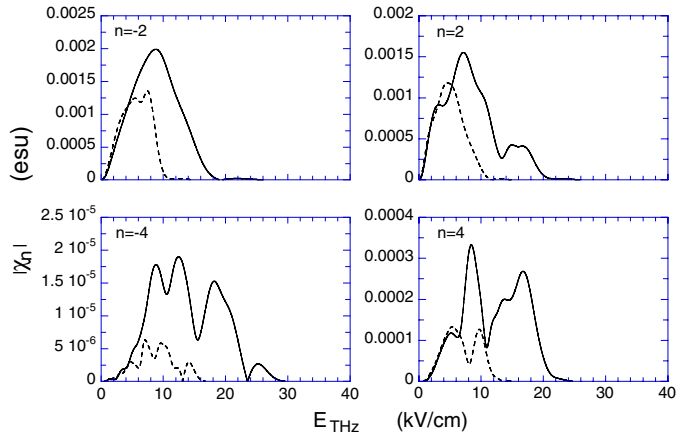

Figure 4. $|\chi|$ versus E_{THz} for various sidebands obtained using the same parameters as for figure 3.

$|\omega - \omega_v|$. Thus $|\chi_n|$ survives up to higher E_{THz} for larger detuning. Also, E_{th} is independent of the sideband index n. All these features are clearly seen in figures 3 and 4.

This REHS also explains the oscillatory variation of χ at intermediate E_{THz}: at a particular instant, the electron and hole are located at different positions and feel different THz potentials. The difference between these potentials oscillates in time, making the recombination photon-assisted. Thus it is no coincidence that figures 3 and 4 resemble the current–voltage characteristics of photon-assisted tunnelling [24]. Bessel functions describe the oscillations in both cases (see equation (B.5*b*)).

In equation (18), Ω is contained only in the denominators, so the dependence on Ω of χ_n is rather simple. In particular, Im χ_0 as a function of Ω consists of a series of Lorentzian peaks centred at $\Omega = \Omega_{nn'l}$. Figure 5 illustrates this for $B = 8.22$ T ($\omega_c = 14.19$ meV) and $\omega = 15$ meV. For $E_{\mathrm{THz}} = 1$ kV cm^{-1} (solid line), the system is still in the low-field regime, i.e., the peaks occur (from left to right) at $\Omega = \Omega_{000}$, Ω_{110}, Ω_{220}, Ω_{330}, and Ω_{440}. As the field increases, other resonances gain intensity and the assignment of a peak to a single $(nn'l)$ resonance loses its meaning. For $E_{\mathrm{THz}} = 10$ kV cm^{-1} (dashed line), each of the peaks is

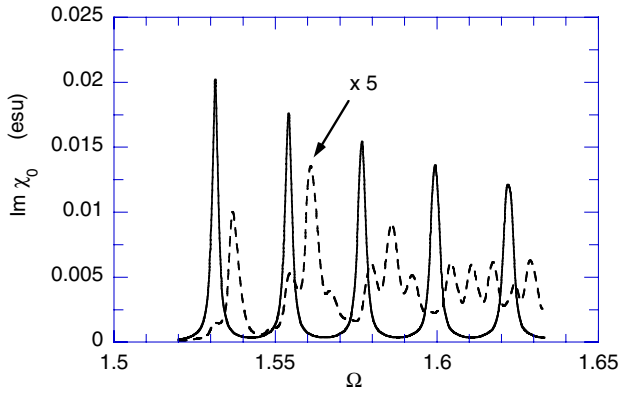

Figure 5. Calculated Im χ_0 versus Ω for $E_{\mathrm{THz}} = 1$ (solid line) and 10 kV cm^{-1} (dashed line). The other parameters are $\omega = 15$ meV and $B = 8.22$ T.

actually a superposition of five to ten resonances ($\Omega = \Omega_{nn'l}$ with different values of $(nn'l)$). Since more resonance channels become available as Ω increases, the overall peak density is greater in the large-Ω region. A close examination of the origins of the peaks has revealed that resonances with $n \gg n'$ are dominant. This may be understood from the fact that $\omega \approx \omega_c$ in this example, and, therefore, the CB electrons can be easily excited to higher LLs.

5. Summary

An analytic, nonperturbative theory of light absorption and scattering (sideband generation) by Landau-quantized electrons and holes driven by intense THz radiation has been developed. The result underlines the importance of resonant electron–hole separation near CR which causes the sideband intensity to oscillate as a function of E_{THz} and decay exponentially to zero as $E_{\mathrm{THz}} \to \infty$. The CR peaks exhibit a dip at their centres, which broaden as $E_{\mathrm{THz}} \to \infty$.

In real systems, intra-LL relaxation, which was neglected in the present work, tends to suppress the REHS. In my previous publication [18], I made a crude estimation of its influence by introducing a phenomenological relaxation time. The result indicated that the predicted REHS-induced effects are still observable as long as the relaxation time is longer than $\approx$0.1 ps. At present, we still lack detailed information about the dephasing time in nanostructures driven by a strong THz field. We look forward to future efforts in this direction.

Acknowledgments

I would like to thank J Kono, H Sakaki and T Ando for valuable discussions.

Appendix A. Driven harmonic oscillator wave functions

To obtain the stationary solutions of the Schrödinger equation:

$$\mathrm{i}\dot{\psi} = H\psi \tag{A.1a}$$

$$H = -\frac{1}{2m}\frac{\partial^2}{\partial x^2} + \frac{1}{2}m\omega_c^2 x^2 + eEx\sin\omega t \tag{A.1b}$$

we introduce a unitary transformation:

$$f(xt) = U\psi(xt) \tag{A.2a}$$

$$U = \mathrm{e}^{-\mathrm{i}m\dot{\gamma}x}\mathrm{e}^{\mathrm{i}\gamma p}. \tag{A.2b}$$

Here

$$\gamma(t) = \frac{eE}{m(\omega^2 - \omega_c^2)}\sin(\omega t) \tag{A.3}$$

is a solution of the classical equation of motion:

$$m\ddot{\gamma} = -m\omega_c^2\gamma - eE\sin(\omega t). \tag{A.4}$$

The new function f satisfies $[U(\mathrm{i}\,\partial/\partial t - H)U^{-1}]f = 0$, or, upon carrying out the unitary transformation and using equation (A.4),

$$\mathrm{i}\dot{f} = -\frac{1}{2m}\frac{\partial^2 f}{\partial x^2} + \frac{1}{2}m\omega_c^2 x^2 f - L(t)f \tag{A.5a}$$

$$L(t) = \frac{m}{2}\dot{\gamma}^2 - \frac{1}{2}m\omega_0^2\gamma^2 - eE\gamma\sin\omega t. \tag{A.5b}$$

($L(t)$ is the Lagrangian for the classical trajectory $\gamma(t)$.) The solutions of equations (A.5) are

$$f_n(xt) = w_n(x)\mathrm{e}^{-\mathrm{i}E_n t}\mathrm{e}^{\mathrm{i}\int_0^t L(s)\,\mathrm{d}s} \tag{A.6}$$

where

$$w_n(x) = \frac{1}{\sqrt{2^n n!}}\left(\frac{m\omega_c}{\pi}\right)^{1/4}\mathrm{e}^{-m\omega_c x^2/2}H_n(\sqrt{m\omega_c}x) \tag{A.7}$$

is a harmonic oscillator eigenfunction and $E_n = (1/2+n)\omega_c$ its energy. ($H_n(x)$ is the Hermite polynomial of order n.) From this we obtain

$$\psi_n(x,t) = U^{-1}f_n(xt) = w_n(x-\gamma)\mathrm{e}^{-\mathrm{i}E_n t}\mathrm{e}^{\mathrm{i}m\dot{\gamma}(x-\gamma)}\mathrm{e}^{\mathrm{i}\int_0^t L(s)\,\mathrm{d}s}. \tag{A.8}$$

Appendix B. Calculation of $Q_{nn'\sigma,\alpha}$

To calculate $\langle\tilde{\psi}_{cnX\sigma}(t)|p_\alpha|\tilde{\psi}_{vn'X'\sigma}(t)\rangle$, we insert equations (7) and (8) into the definition and use the identity

$$\frac{1}{L_y}\int_{-L_y/2}^{L_y/2}\mathrm{d}y\;\mathrm{e}^{\mathrm{i}(X-X')y/\ell^2} = \delta_{XX'} \tag{B.1}$$

to obtain

$$\langle\tilde{\psi}_{cnX\sigma}(t)|p_\alpha|\tilde{\psi}_{vn'X'\sigma}(t)\rangle = \delta_{XX'}Q_{nn'\sigma,\alpha} \tag{B.2}$$

with

$$Q_{nn'\sigma,\alpha} = \langle\Phi_{c\sigma}|p_\alpha|\Phi_{v\sigma}\rangle\mathrm{e}^{\mathrm{i}(\bar{E}_{cn}-\bar{E}_{vn'})t}F_{nn'}(t) \tag{B.3a}$$

$$F_{nn'}(t) = \int_{-\infty}^{\infty}\mathrm{d}x\;w_{cn}(x-\gamma_c)w_{vn'}(x-\gamma_v)\mathrm{e}^{-\mathrm{i}G_{cX}(xt)+\mathrm{i}G_{vX}(xt)}. \tag{B.3b}$$

Performing the x-integration and using

$$\mathrm{e}^{\mathrm{i}a\sin 2\omega t + b\cos 2\omega t} = \sum_{l=-\infty}^{\infty}J_l\left(\sqrt{a^2-b^2}\right)\left(\frac{a+b}{\sqrt{a^2-b^2}}\right)^l\mathrm{e}^{2\mathrm{i}l\omega t} \tag{B.4}$$

where $J_l(z)$ is the Bessel function of order l, we finally obtain

$$Q_{nn'\sigma,\alpha} = \langle \Phi_{c\sigma}|p_\alpha|\Phi_{v\sigma}\rangle \mathrm{e}^{\mathrm{i}(\bar{E}_{cn}-\bar{E}_{vn'})t} \sum_{l=-\infty}^{\infty}{}^{(n-n')} \mathrm{e}^{-\mathrm{i}l\omega t} D(l,n,n') \tag{B.5a}$$

$$D(l,n,n') = \mathrm{e}^{-(\Delta^2+\omega^2\Gamma^2)/8} \sum_{M=-n_2}^{n_1} A_1(n,n',M) J_{M-(l+n_1-n_2)/2}\left(\sqrt{A_2^2-A_3^2}\right) \times \left(\frac{A_2+A_3}{\sqrt{A_2^2-A_3^2}}\right)^{M-(l+n_1-n_2)/2} \tag{B.5b}$$

$$A_1(n,n',M) = \sqrt{\frac{2^{n_2}n_2!}{2^{n_1}n_1!}} \sum_{k_3=\max(-M,0,M-n_1+n_2)}^{n_2} \sum_{k_2=0}^{k_3} \sum_{k_1=0}^{n_1-n_2} \binom{n_1}{n_2-k_3}\binom{k_3}{k_2}\binom{n_1-n_2}{k_1} \times \frac{(\omega\Gamma)^{k_1+2k_2}\Delta^{n_1-n_2-k_1-2k_2+2k_3}[\sigma_{n'n}]^{n_1-n_2-k_1}}{k_3!2^{n_1-n_2+3k_3}\mathrm{i}^{n_1-n_2-2k_1-2k_2}} \times \eta(k_3+M, n_1-n_2-k_1-2k_2+2k_3, k_1+2k_2) \tag{B.5c}$$

$$A_2 = \frac{e^2E_{\mathrm{THz}}^2[m_c(\omega^2+\omega_c^2)+m_v(\omega^2+\omega_c^2)]}{8m_cm_v\omega(\omega^2-\omega_c^2)(\omega^2-\omega_v^2)} \tag{B.5d}$$

$$A_3 = \frac{e^2E_{\mathrm{THz}}^2\ell^2(\omega_c+\omega_v)^2}{8(\omega^2-\omega_c^2)(\omega^2-\omega_v^2)} \tag{B.5e}$$

$$\Gamma = eE_{\mathrm{THz}}\ell\left(\frac{1}{\omega^2-\omega_v^2}-\frac{1}{\omega^2-\omega_c^2}\right) \tag{B.5f}$$

$$\Delta = \frac{eE_{\mathrm{THz}}}{\ell}\left(\frac{1}{m_v(\omega^2-\omega_v^2)}-\frac{1}{m_c(\omega^2-\omega_c^2)}\right) \tag{B.5g}$$

$$\eta(k_1,k_2,k_3) = \sum_{l=\max(0,k_1-k_3)}^{\min(k_1,k_2)} (-1)^l \binom{k_2}{l}\binom{k_3}{k_1-l} \tag{B.5h}$$

where $n_1 = \max(n,n')$, $n_2 = \min(n,n')$, and $\sigma_{n'n} = 1$ if $n' \geqslant n$ and -1 otherwise. Furthermore, in equation (B.5a), the l-summation runs over even (odd) integers if $(n-n')$ is even (odd), and $\bar{E}_{cn}$ and $\bar{E}_{vn}$ are defined by equations (7c) and (8c), respectively.

References

[1] Kono J, Černe J, Inoshita T, Sherwin M S, Sundaram M and Gossard A C 1996 *Proc. 23rd Int. Conf. on the Physics of Semiconductors* ed M Scheffler and R Zimmermann (Singapore: World Scientific) p 1911

[2] Kono J, Inoshita T, Sakaki H, Černe J, Sherwin M S, Sundaram M and Gossard A C 1997 *High Magnetic Fields in the Physics of Semiconductors II* ed G Landwehr and W Ossau (Singapore: World Scientific) p 785

[3] Černe J, Kono J, Inoshita T, Sherwin M, Sundaram M and Gossard A C 1997 *Appl. Phys. Lett.* **70** 3543

[4] Kono J, Su M Y, Nordstrom K B, Černe J, Sherwin M S, Allen S J, Noda, Inoshita T and Sakaki H 1997 *Proc. SPIE* **3153** 96

[5] Kono J, Su M Y, Inoshita T, Noda T, Sherwin M S, Allen S J and Sakaki H 1997 *Phys. Rev. Lett.* **79** 1758

[6] Chin A H, Carderon A H and Kono J 2001 *Phys. Rev. Lett.* **86** 3292

[7] Phillips C, Su M Y, Sherwin M S, Ko J and Coldren L 1999 *Appl. Phys. Lett.* **75** 2728

[8] Zudov M A, Kono J, Mitchell A P and Chin A H 2001 to be published

[9] Nordstrom K B, Johnsen K, Allen S J, Jauho A-P, Birnir B, Kono J, Noda T, Akiyama H and Sakaki H 1997 *Phys. Status Solidi* b **204** 52

[10] Nordstrom K B, Johnsen K, Allen S J, Jauho A-P, Birnir B, Kono J, Noda T, Akiyama H and Sakaki H 1998 *Phys. Rev. Lett.* **81** 457

[11] Yacoby Y 1968 *Phys. Rev.* **169** 610

[12] Jauho A P and Johnsen K 1996 *Phys. Rev. Lett.* **76** 4576
[13] Johnsen K and Jauho A P 1998 *Phys. Rev.* B **57** 8860
[14] Johnsen K and Jauho A P 1999 *Phys. Rev. Lett.* **83** 1207
[15] Inoshita T, Kono J and Sakaki H 1998 *Phys. Rev.* B **57** 4604
[16] Inoshita T and Sakaki H 1998 *Physica* B **249–251** 534
[17] Inoshita T and Sakaki H 1999 *Proc. 24th Int. Conf. on the Physics of Semiconductors* ed D Gershoni (Singapore: World Scientific) CD-ROM 0085.pdf
[18] Inoshita T 2000 *Phys. Rev.* B **61** 15 610
[19] Yu P Y and Cardona M 1996 *Fundamentals of Semiconductors* (Berlin: Springer) section 9.2
[20] The time evolution operator for the problem was obtained by
Hawrylak P and Rego L 1998 *Physica* E **3** 198
[21] See, for example,
Aoki H and Kamimura H 1989 *The Physics of Interacting Electrons in Disordered Systems* (Oxford: Oxford University Press) ch 5
[22] See, for example,
Cohen-Tannoudji C, Dupont-Roc J and Grynberg G 1992 *Atom–Photon Interactions* (New York: Wiley)
[23] Yu P Y and Cardona M 1996 *Fundamentals of Semiconductors* (Berlin: Springer) p 69
[24] For a review, see
Allen S J, Bhattacharya U, Campman K, Drexler H, Gossard A, Keay B J, Maranowski K, Medeiros-Ribero G, Rodwell M, Scott J S, Unterrainer C, Wanke M and Zeuner S 1996 *Physica* B **227** 367